# EXCIMER LASERS

A.J. Palmer and L.D. Hess

Hughes Research Laboratories
3011 Malibu Canyon Road
Malibu, CA 90265

June 1976

DARPA Order No.     1807

Program Code No.    6E20

Contractor       Hughes Research Laboratories

Effective Date of Contract  1 October 1974

Contract Expiration Date  15 November 1976

Amount of Contract    $298,989.00

Contract No.       N00014-75-C-0081

Principal Investigator   A. Jay Palmer

Telephone No.      (213) 456-6411, extension 356

Title of Work      Excimer Lasers
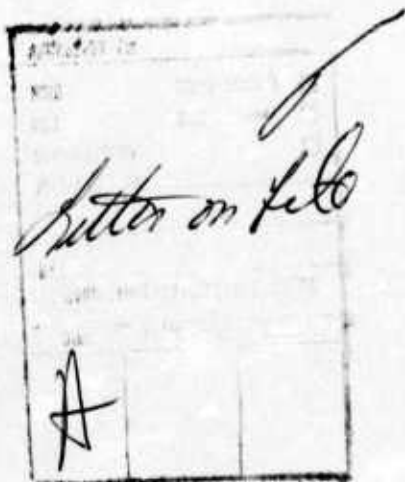
| REPORT DOCUMENTATION PAGE | | READ INSTRUCTIONS BEFORE COMPLETING FORM |
|---|---|---|
| 1. REPORT NUMBER *(9) Semiannual technical rept. no. 3, 1 Oct 75-31 Mar 76* | 2. GOVT ACCESSION NO. | 3. RECIPIENT'S CATALOG NUMBER |
| 4. TITLE (and Subtitle) *(6)* EXCIMER LASERS | | 5. TYPE OF REPORT & PERIOD COVERED Semiannual Tech. Rpt. 3 1 Oct. 1975 - 31 Mar. 1976 |
| | | 6. PERFORMING ORG. REPORT NUMBER |
| 7. AUTHOR(s) *(10)* A. J. Palmer and L. D. Hess | *(15)* | 8. CONTRACT OR GRANT NUMBER(s) N00014-75-C-0081 |
| 9. PERFORMING ORGANIZATION NAME AND ADDRESS Hughes Research Laboratories 3011 Malibu Canyon Road Malibu, CA 90265 | | 10. PROGRAM ELEMENT, PROJECT, TASK AREA & WORK UNIT NUMBERS ARPA Order No. 1807 Program Code No. 6E20 |
| 11. CONTROLLING OFFICE NAME AND ADDRESS Defense Advanced Research Projects Agency Arlington, VA 22209 | *(11)* | 12. REPORT DATE June 1976 |
| | | 13. NUMBER OF PAGES 48 |
| 14. MONITORING AGENCY NAME & ADDRESS(if different from Controlling Office) Office of Naval Research 800 N. Quincy Street Arlington, VA 22217 *(12) 50p.* | | 15. SECURITY CLASS. (of this report) Unclassified |
| | | 15a. DECLASSIFICATION DOWNGRADING SCHEDULE |

16. DISTRIBUTION STATEMENT (of this Report)

DISTRIBUTION STATEMENT A
Approved for public release;
Distribution Unlimited

17. DISTRIBUTION STATEMENT (of the abstract entered in Block 20, if different from Report)

18. SUPPLEMENTARY NOTES

19. KEY WORDS (Continue on reverse side if necessary and identify by block number)

Excimer Lasers, Dimer Lasers, Alkali-Rare Gas Lasers, Continuum Lasers

20. ABSTRACT (Continue on reverse side if necessary and identify by block number)

The primary goals of this program are to identify specific operating conditions for achieving laser oscillation on the A to X transitions of the diatomic alkali-rare gas excimer molecules (excimers) and of the diatomic homonuclear alkali moledule (dimers) and to demonstrate net laser gain in a laboratory experiment from at least one of the alkali-rare gas systems. → OVER

DD FORM 1473 EDITION OF 1 NOV 65 IS OBSOLETE

172 600

The phase of the program covered by this report was devoted to experiments and theoretical modeling on discharge pumping of the potassium-xenon and potassium-argon excimer-dimer systems.

A time dependent discharge model was developed and is being used to predict discharge and stimulated emission characteristics of a pulsed transverse discharge through potassium-argon and potassium-xenon mixtures. Modeling results show stable discharge operation under conditions which yield a practical laser gain coefficient on both the K-Xe and K-Ar excimer bands and on the $K_2$ dimer band. Specifically, gain coefficients on the order of $10^{-22}$ cm$^{-1}$ are predicted on the K-Xe or K-Ar excimer bands at $250°$ with [Xe] (or [Ar]) $\approx 10^{20}$ cm$^{-3}$ at a current density of $\sim 0.1$ A/cm$^2$. Similar values of the gain coefficient on the $K_2$ dimer band are predicted at $300°$C, [Xe] (or [Ar]) $\approx 1 \times 10^{20}$ cm$^{-3}$, and at a current density of 0.2 A/cm$^2$.

A discharge apparatus containing transverse electrodes with a 2 cm x 13.5 cm area and a 1 cm gap has been fabricated which is capable of operation at total pressures up to 10 atm and a temperature of $350°$C. Methods for obtaining "aerosol-free" mixtures of potassium and argon have been developed. A diffuse discharge was achieved with a mixture of potassium and argon at 100 psia and $250°$C. Discharge electrical and spectral measurements were carried out under a variety of experimental conditions and are reported herein.

# TABLE OF CONTENTS

BLANK PAGE

## LIST OF ILLUSTRATIONS

# I.   INTRODUCTION

This is the third semiannual technical report on the ARPA/ONR program to develop high energy alkali-rare gas excimer/dimer lasers. The primary goals of this program are to identify specific operating conditions for achieving laser oscillation on the A to X transitions of the diatomic alkali-xenon excimer molecules (excimers) and of the diatomic homonuclear alkali molecule (dimers), and to demonstrate net laser gain in a laboratory experiment from at least one of the alkali-xenon systems.

During the first year period of this program the primary accomplishments were as follows:

1.   The development of a theoretical model which computes the small-signal gain for all of the alkali-xenon excimer/dimer systems for flashlamp optical pumping.

2.   The construction of a one meter long high temperature, high pressure optically pumped potassium xenon experimental cell.

3.   Experimental determination of the absorption coefficient on the K-Xe excimer and $K_2$ dimer band and of the stimulated emission coefficient on the K-Xe excimer band all of which were consistent with the modeling.

4.   The achievement of preliminary observations of low pressure discharge pumped fluorescence spectra of the K-Ar excimer and dimer bands.

Several attempts at achieving laser oscillation on both the excimer and dimer bands in the optically pumped K-Xe tube were made during this first year period and during the early part of the present reporting period. Lasing was not achieved and is attributed to a combination of factors including optical loss due to the presence of aerosols and refractive index inhomogeneities, a lack of adequate flashlamp brightness, and a possible collisional quenching of the dimer emission. Time did not permit any of these factors to be given adequate study in the

optically pumped experiments in order to quantitatively assess their influence on the net laser gain before the shift to present discharge pumping experiments was implemented.

Beginning with the present reporting period we have shifted from optical pumping to transverse discharge pumping as the means to demonstrate efficient scalable laser oscillation of an alkali-rare gas excimer/dimer system. Accomplishments made during this reporting period include (1) the development of a completely time dependent theoretical model for discharge pumping of the K-Xe excimer/dimer system, (2) the construction of a transverse discharge tube utilizing a 1 cm x 2 cm x 13.5 cm discharge volume and a flashlamp preionizer, (3) the apparent elimination of aerosol formation in this tube, and (4) the achievement of a diffuse discharge through a potassium-argon mixture at $\sim 200^{\circ}$C and a pressure of 7 atmospheres. Peak currents up to 300 A were observed at a discharge voltage of 1 kV/cm which corresponds to a discharge power loading of 11 kW/cm$^3$. The current status of the theoretical and experimental activities are presented in Sections II and III, respectively. Section IV presents the anticipated work plan for the next six month reporting period during which we anticipate achieving laser oscillation in the present diffuse discharge.

## II.   THEORETICAL  PROGRAM

### A.   Time Dependent Discharge Model

Both the optical pumping and discharge pumping models presented in the reports prior to this one were steady state models. Steady state modeling is justifiable for optical pumping since there the relaxation times of all optical pumping and kinetics processes are short compared to the flashlamp pulse duration. On the other hand, this is generally not the case for discharge pumping. In particular, such discharges tend to be unstable and it is not a priori clear that a steady state discharge mode can be reached at any time. Thus, the original steady state discharge model discussed in the previous report serves only as a preliminary estimate of operating conditions for achieving laser threshold. A full time dependent discharge model is presented below.

The new discharge model follows the time evolution in the discharge of the concentration of six excited and ionized alkali states, the electron and gas temperatures, and the net small-signal gain coefficient at two wavelengths, one near the peak of the excimer gain band, and the other at the dimer satellite wavelength. The time dependence of the circuit current and voltages is also included with a series resistance, a series inductance, and a storage capacitor as the modeled circuit elements.

The plasma and gas kinetic processes included in the rate equations governing the species concentrations are listed below. The rate constants, cross-sections, and equilibrium constants for these processes can be found in the computer code listing included in Appendix A, and, together with a source reference, in Table II-1. An R label refers to a plasma process while a G label refers to a gas kinetic process. In the listing, a B at the end of the label refers to the back reaction which is computed by detailed balancing using the appropriate equilibrium constant or Boltzmann factor reaction. The particular case presented refers to a potassium-xenon mixture.

9

## Table II-1. List of Cross-Sections, Rate Constants, Equilibrium Constants and Source References used for Discharge Pumped K-Xe/K₂ Modeling

| Parameter | Value | Reference |
|---|---|---|
| Inelastic electron collision cross-sections: initial slope of cross-sections w.r.t. energy above threshold | | |
| CPI | $6 \times 10^{-15}$ cm$^2$/eV | 3 |
| CPI | $0.5 \times 10^{-16}$ cm$^2$/eV | 3 |
| CPII | $5 \times 10^{-16}$ cm$^2$/eV | Rough Estimate |
| Recombination coefficients: | | |
| Three-body RECP | $2.28 \times 10^{-26} \times [K^+] \times [Ne]^2 \times Te^{(-4.39)}$ cm$^{-3}$ sec$^{-1}$ | 5 (Cesium) Rough Estimate |
| Dissociative — (K Xe$^+$) RECPX | $3.3 \times 10^{-5} \times [K] \times [Xe^+] \times [Ne] \times Te^{(-0.67)}$ cm$^{-3}$ sec$^{-1}$ | |
| Dissociative — (K$_2^+$) RECPD | $3.3 \times 10^{-5} \times [K_2^+] \times [Ne] \times Te^{(-0.67)}$ cm$^{-3}$ sec$^{-1}$ | Rough Estimate |
| Photoionization Cross-Section: CPHI | $0.5 \times 10^{-19}$ cm$^2$ | 4 |
| Electron Elastic Cross-Section: CEL | $5.5 \times 10^{-16}$ cm$^2$ | 3 |
| Heavy Particle Elastic Cross-Section: CDIF | $1 \times 10^{-15}$ cm$^2$ | Rough Estimate |
| Gas Kinetic Rates: GPD | $8 \times 10^{-32} \times [Xe] \times [K] \times [K*]$ cm$^{-3}$ sec$^{-1}$ | 6 |
| Equilibrium Constants: | | |
| KAEX | $2.2 \times 10^{-23} \times \exp(0.074/Tg)$ cm$^3$ | 7 (Rubidium) |
| KXDI | $1.8 \times 10^{-22} \times \exp(0.56/Tg)$ cm$^3$ | 6 |
| KADI | $6.5 \times 10^{-23} \times \exp(0.735/Tg)$ cm$^3$ | 6 |
| Optical Rates All radiative rates, absorptive and stimulated emission cross-sections and their dependences on temperature and density are taken from Reference 2. | | |

T1926

The plasma processes modeled are:

| | | | |
|---|---|---|---|
| RPI: | $e^- + K$ | $\rightarrow$ | $K^+ + 2e^-$ |
| RP1: | $e^- + K$ | $\rightleftharpoons$ | $K^* + e^-$ |
| RPII: | $e^- + K^*$ | $\rightarrow$ | $K^+ + 2e^-$ |
| RECP: | $e^- + K^+ + e^-$ | $\rightarrow$ | $K^* + e^-$ |
| RECPX: | $e^- + K Xe^+$ | $\rightarrow$ | $K^* + Xe$ |
| RECPD: | $e^- + K_2^+$ | $\rightarrow$ | $K^* + K$ |
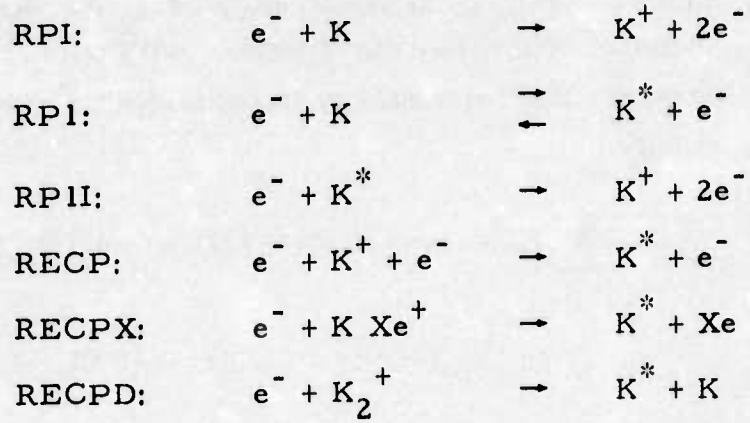
The gas kinetic processes modeled are:

| | | | |
|---|---|---|---|
| GPX: | $K + 2 Xe$ | $\rightleftharpoons$ | $K Xe + Xe$ |
| GPD: | $K + K + Xe$ | $\rightleftharpoons$ | $K_2 + Xe$ |
| GPX1: | $K^* + 2 Xe$ | $\rightleftharpoons$ | $K Xe^* + Xe$ |
| GPD1: | $K^* + K + Xe$ | $\rightleftharpoons$ | $K_2^* + Xe$ |
| GPXI: | $K^+ + 2 Xe$ | $\rightleftharpoons$ | $K Xe^+ + Xe$ |
| GPDI: | $K^+ + K + Xe$ | $\rightleftharpoons$ | $K_2^+ + Xe$ |
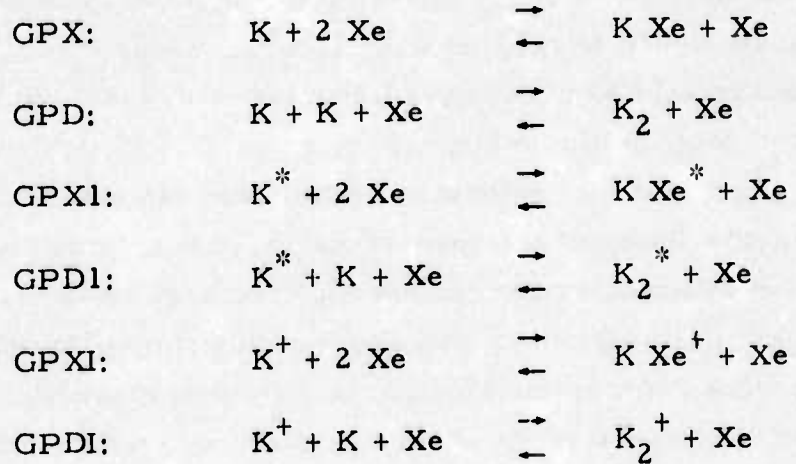
The radiative processes modeled are:

| | | | |
|---|---|---|---|
| AT: | $K^*$ | $\rightarrow$ | $K + h\nu$ (TRAPPED) |
| AP: | $K^{**}$ | $\rightarrow$ | $K + h\nu$ |
| AP: | $KXe^*$ | $\rightarrow$ | $KXe + h\nu$ |
| AP: | $K_2^*$ | $\rightarrow$ | $K_2 + h\nu$ |
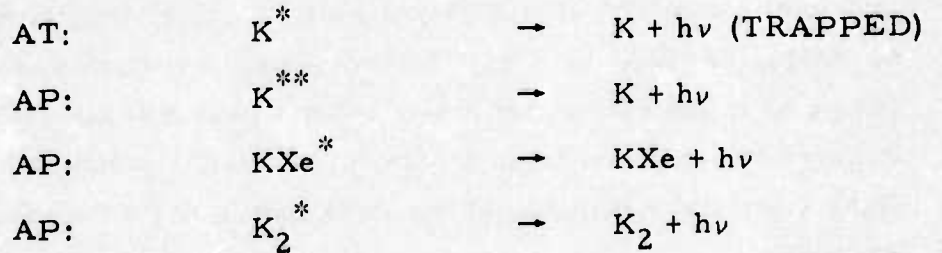
Under the conditions we consider $\left([Xe] \approx 1 \times 10^{20} \ cm^{-3}\right)$ the gas kinetic rates dominate over electron collisional rates in controlling the population of the molecular states. We therefore assume thermal equilibrium at the gas temperature to be maintained between the

11

molecular states and their dissociation products. As in the optical pumping model an exception is the A-state of $K_2$ for which radiative losses are included since they can compete with the dissociation rate.

The average electron energy is computed by solving the electron energy equation:

$$
J \bullet E_{disch} = \sum_i (\text{INELASTIC COLLISION RATE } (Te))_i \times E_i
$$

$$
+ (\text{ELASTIC COLLISION RATE}) \times 2 \left( \frac{Me}{M_m} \right) \times Te \tag{1}
$$

where J is the current density, $E_{disch}$ is the discharge electric field, $E_i$ is the inelastic energy loss for the $i^{th}$ process and $M_m$ and $M_e$ are the masses of the M species and electron, respectively. At present the resonance level pumping is assumed to be the dominate inelastic process contributing to the energy equation. For this reason together with the fact that the molecular association rates which pump the upper laser levels dominate the loss of the resonance level population, the predicted efficiencies for converting discharge power to laser power is essentially the quantum efficiency of the transition which is lasing. A Maxwellian energy distribution is assumed at present and will eventually be replaced by an energy distribution arrived at by solving the Boltzman equation. The Maxwell distribution should be a fair approximation because of the dominance of two-step alkali ionization processes over the single step alkali ionization under the considered operating conditions. Only the latter process requires electrons with energies in the tail of the distribution where a large reduction of the number of electrons from a Maxwellian distribution is known to occur. Excitation and ionization of the rare gas is neglected entirely for this reason.

The electron collisional rate constants are expressed, as in the previous report, in a form which results from assuming a linear rise of the cross-section with energy above threshold.[1]

$$R(Te) = \frac{6 \cdot 10^2}{(e/m_e)/\pi} \left.\frac{d\sigma}{d\epsilon}\right|_{\epsilon_0} \left(\frac{2}{m_e} Te\right)^{3/2} \exp(-\epsilon_0/Te)\left(1 + \frac{\epsilon_0}{2Te}\right) \quad (2)$$

where $\epsilon_0$ is the threshold energy for the excitation or ionization process. $d\sigma/d\epsilon_{\epsilon_0}$ is the rat of rise of cross-section with energy above threshold and $m_e$ and e is the electron mass and change.

Also, in solving eq. (1) we use an expression for the drift velocity obtained from Ref. 1

$$V_{drift} = (2 Te/M_{Xe})^{1/2} \quad (3)$$

where $M_{Xe}$ is the mass of the xenon atoms.

The gas temperature is calculated by assuming that all of the discharge power goes into gas heating and that heat is removed only by thermal conduction to a wall (assumed cylindrical).

$$\frac{d T_G}{dt} = J \bullet E_{disch}/(3/2 [M]) - (\text{THERMAL CONDUCTIVITY})$$

$$\times \left(\frac{4.8}{\text{DIAMETER}}\right)^2 \times \left(T_G - T_{WALL}\right) \quad (4)$$

The discharge circuit response is governed by the familiar circuit equations.

$$V_{disch} = V_c(t) - L \times \frac{dI}{dt} - R \times I \quad (5)$$

$$V_c(t) = V_{charge} - 1/C \int I\, dt \quad (6)$$

where $V_{disch}$ is the discharge voltage, $V_c$ is the capacitor voltage, $V_{charge}$ is the initial charging voltage, I is the discharge current, and R, L, and C are the series resistance, inductance, and storage capacitance, respectively.

$$\text{GAIN}(\lambda) = \sigma_{\text{STIM, ex}}(\lambda) \left\{ [KXe^*] \times \frac{\exp(-V_{A, Ex}(\lambda)/T_G)}{(K_{eq\,A, Ex} \times 3/2)} \right.$$

$$\left. - 2 \times [K] \times [Xe] \times \exp(-V_{x, Ex}(\lambda)/T_G) \right\}$$

$$+ \sigma_{\text{STIM, Di}}(\lambda) \left\{ [K_2^*] \times \frac{\exp(-V_{A, Di}(\lambda)/T_G)}{(K_{eq\,A, Di} \times 12)} \right.$$

$$\left. - 0.25 \times [K]^2 \times \exp(-V_{x, Di}(\lambda)/T_G) \right\} \tag{7}$$

$$\sigma_{\text{STIM}}(\lambda)_{\substack{Ex \\ Di}} = (A_E/2c) \times \lambda^2 \times R_{\substack{Ex \\ Di}}^2 \times \left. \frac{dR(\lambda)}{d\nu} \right|_{\substack{Ex \\ Di}} \tag{8}$$

where the notation follows that used in Ref. 2.

As shown by the computer code listing, the coupled rate equations governing all of the above processes are integrated numerically using a time step chosen by the user and altered, if desired, during the course of the computer run. The computer program is written for the PDP10 computer.

## B.   Results and Discussions

The results of three computer runs of the above model are presented in Figs. II-1 through II-3. The series inductance, L, and resistance, R, are assumed equal to zero in these runs.

The two results presented in Fig. II-1 are for an avalanche discharge through a 10 atm potassium-xenon mixture at two different temperatures. As in the optical pumping case, the lower temperature result shows most of the gain occurring on the excimer band (8500 Å), while the higher temperature case shows the highest gain occurring on the dimer hand. In both cases the model predicts that a fairly high E/N value of $\sim 10^{-11}$ V/(cm·[K] cm$^{-3}$) is required to give practical gain

14

coefficients of ~1%/cm. The much lower E/N values in the steady state discharge modeling results presented in the last semiannual report were due primarily to the erroneous neglect of dissociative recombination channels for the alkali ions and to a lesser extent to a poor approximation used therein for the drift velocity.

The results in Fig. II-1 are for an infinite storage capacitance, and illustrate an important feature of the discharge kinetics. Unlike the other popular class of discharge pumped excimer systems, the rare gas monohalides, the alkali rare gas discharge appears in the modeling, to be stable against ionization instabilities. This is due to two causes: first, to the fact that the discharge is recombination stabilized rather than attachment stabilized; and second, to the fact ground state potassium population is depleted during the discharge resulting in a saturation of the ionization.

Results for a uv-sustained K-Xe discharge are presented in Fig. II-2. Here a comparable dimer gain coefficient is achieved at half the discharge E/N value required dor the 300° avalanche discharge case. Very high flashlamp brightness is required here and results in an extremely low overall efficiency. Since the higher efficiency avalanche discharge is predicted to be stable, there is no apparent advantage in operating the discharge in this mode.

Finally, in Fig. II-3 we present modeling results for a K-Ar discharge with a finite storage capacitance at conditions near those achieved in the current experiments. The potassium density is seen to be too low to yield a practical gain coefficient in this case. We also note that the model results show approximately an order of magnitude lower peak current density than was measured in the experiment at this voltage and capacitance. Tentatively, we attribute this to too high a value estimated for the dissociative recombination rates used in the model. We plan to adjust this rate to match the measured discharge characteristics during the forthcoming phase of experimental measurements.

$[Xe] = 1 \times 10^{20}\,cm^{-3}$

$C = \infty$

$\Phi_{u.v.} = 0$

**Panel a:**

$T_g = 250\,^{\circ}C$
$E_{disch} = 10\,kV/cm$

$J\,(\times 10^{-2}\,A/cm^2)$

GAIN (8,500 Å) $(\times 10^{-3}\,cm^{-1})$

$[K_g]\,(\times 10^{14}\,cm^{-3})$

$[K^*]\,(\times 10^{14}\,cm^{-3})$

GAIN (10,400 Å) $(\times 10^{-3}\,cm^{-1})$

RELATIVE UNITS

a

**Panel b:**

$T_g = 300\,^{\circ}C$
$E_{disch} = 40\,kV/cm$

GAIN (10,400 Å) $\times 10^{-3}\,cm^{-1}$

GAIN (8,500 Å) $(\times 10^{-3}\,cm^{-1})$

$[K_g]\,(\times 10^{15}\,cm^{-3})$

$J\,(\times 10^{-1}\,A/cm^2)$

$[K^*]\,(\times 10^{15}\,cm^{-3})$

t, μsec

b
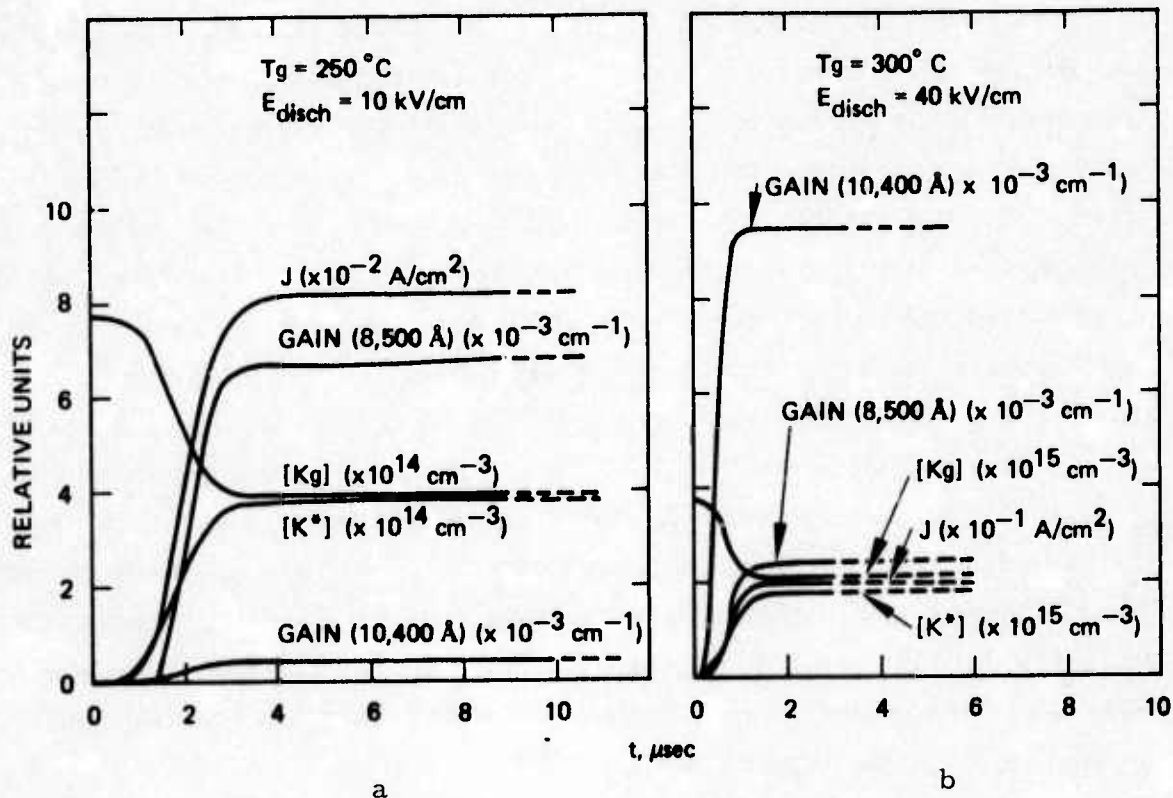
Fig. II-1.  Theoretical modeling results for avalanche sustained discharge pumping of the K-Xe/K$_2$ system.  (a) Low temperature results.  (b) High temperature results.

RELATIVE UNITS

14

12

10

8

6

4

2

0

$[Xe] = 1 \times 10^{20} \, cm^{-3}$

$T_g = 300°C \, ([K] = 3.8 \times 10^{15} \, cm^{-3})$

$C = \infty$

UV Flux $(\times 10^4 \, W/cm^2 \cdot \mu m)$

GAIN (10,400 Å) $(\times 10^{-3} \, cm^{-1})$

$J \, (\times 10^{-3} \, A/cm^2)$
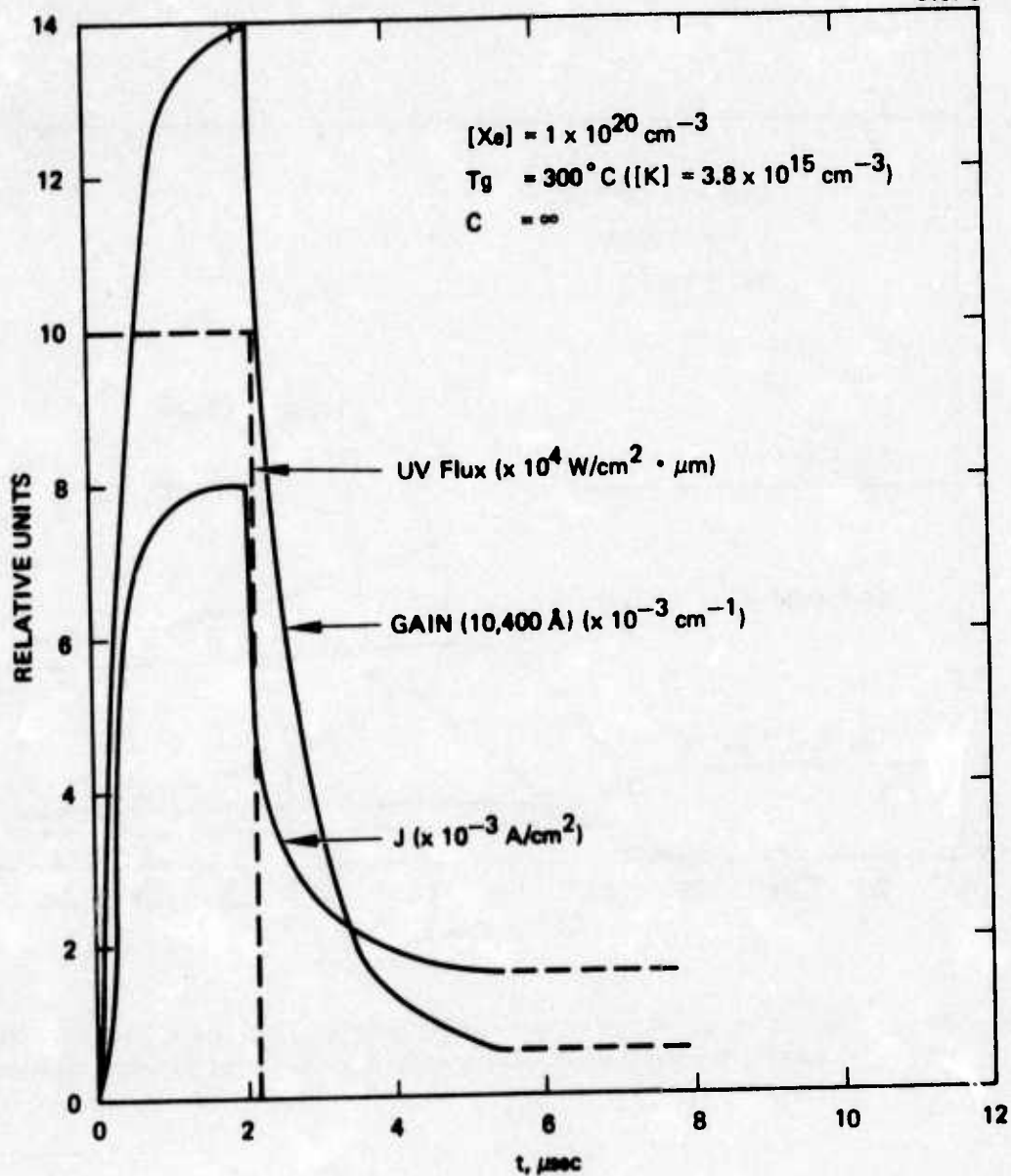
0     2     4     6     8     10     12

t, μsec

Fig. II-2.   Theoretical modeling results for uv sustained dis-
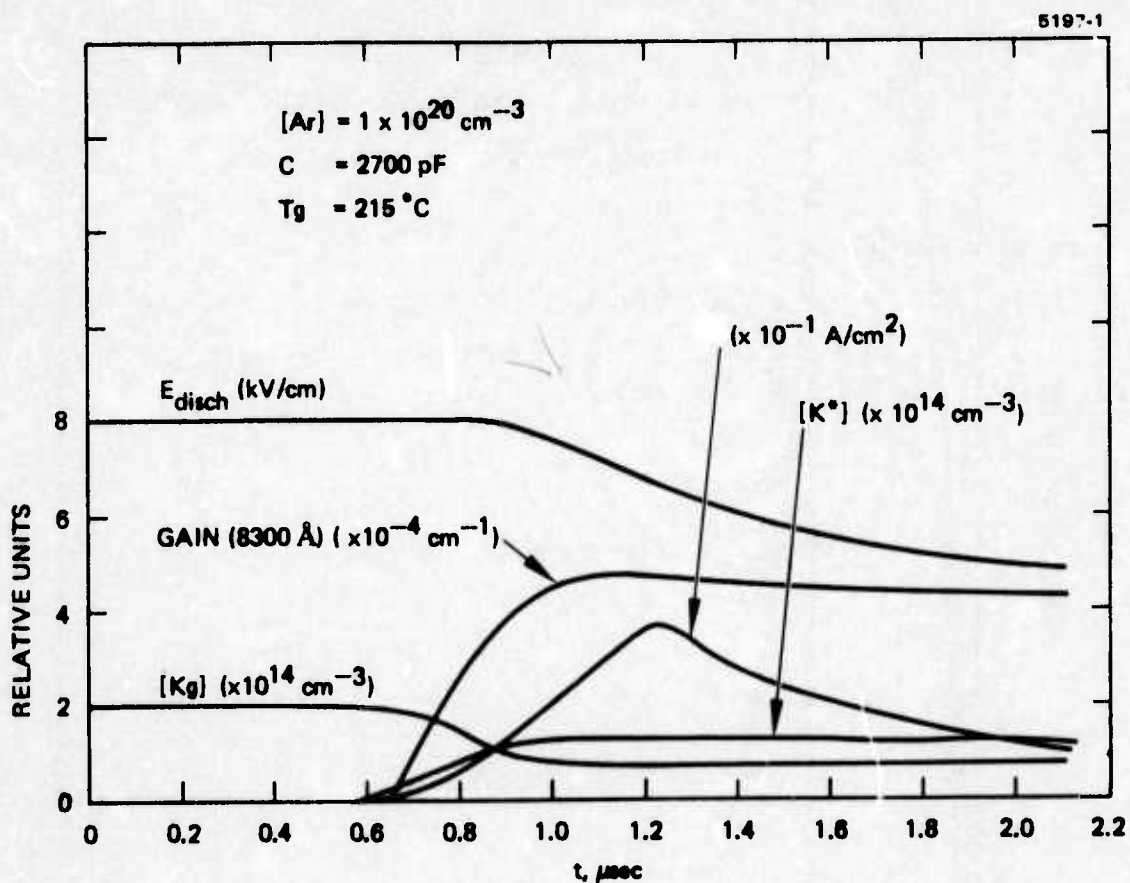charge pumping of the $K-Xe/K_2$ system.

17

Fig. II-3. Theoretical modeling results for avalanche sustained discharge pumping of K-Ar system under conditions achieved in recent experiments.

# III. EXPERIMENTAL PROGRAM

The primary emphasis of the experimental part of the program during this period has been directed toward the achievement of a diffuse discharge in potassium-argon mixtures at high pressure. The discharge dimensions and configuration were chosen in order to obtain experimental results which are directly applicable to scaling considerations for high power laser applications. Thus the discharge apparatus was designed around a transverse electrode arrangement with the width to gap ratio equal to two and the length to gap ratio equal to ten.

In addition to design and fabrication of the electrode apparatus, considerable attention was devoted to solution of the "aerosol" problem encountered in our previous work. Experiments were conducted in a carefully controlled environment under a variety of experimental conditions which have demonstrated that "aerosol-free" mixtures of potassium and argon can be obtained at elevated temperatures and pressures provided temperature gradients are minimized and the potassium vapor is evolved at low pressure. Some of our experiments indicate that the former requirement is more important than the latter.

During the latter part of this reporting period we have achieved a diffuse discharge in a potassium-argon mixture at high pressure (7 atm). The details of these first experiments will be discussed in the following section but it is noteworthy that this discharge has very good spatial homogeneity, exhibits strong K-Ar excimer emission and that no form of auxiliary preionization was required. Potassium atom densities utilized to date are not high enough to provide significant optical gain; however, apparatus modifications are presently underway which will allow the achievement of equilibrium potassium vapor densities at temperatures up to $350^\circ$C. Recent measurements indicate that inadvertent heat transfer through mounting apparatus has restricted the maximum oven temperature to $250^\circ$C.

## A.  Discharge Apparatus

A major concern in the apparatus design was the electrode size and configuration.  An electrode size of 2 cm x 13.5 cm with a gap spacing of 1 cm was chosen initially because it is small enough to be convenient but also large enough to give meaningful results in terms of scaling the system for high power laser applications.  In order to allow maximum flexibility in choice of discharge mode for optimum laser operation we have included provisions in the apparatus for a high intensity flashlamp.  This provides the option of discharge operation in a uv preionized mode, a uv-sustained mode or simply as an over-voltaged avalanche discharge without preconditioning.  A diagram of the first version of this system is shown in Fig. III-1.  A pyrex pressure vessel was selected to provide maximum viewing capability of the discharge.  This design proved to be too difficult to fabricate, however, so an alternate apparatus utilizing a stainless steel pressure vessel with a pyrex liner for electrical isolation was designed and assembled.  This apparatus is illustrated in Fig. III-2 where the electrodes, re-entrant Brewster angle windows, and a large side window for viewing the discharge along its entire length are shown.  This apparatus met the high pressure (10 atm) and discharge viewing requirements but problems developed with the "O" ring seals after several temperature cycles between $25^{\circ}$C and $350^{\circ}$C.  Chemical reactions between several of the components caused difficulties, and thermal gradients contributed to aerosol formation.  This system was revised with the use of metal vacuum flanges and elimination of the pyrex liner.  A photograph of this apparatus is shown in Fig. III-3.  Chemical corrosion problems were virtually eliminated as well as aerosol formation in the new apparatus.  A compromise was made on discharge viewing length because of the maximum window size available with a metal seal; additional windows can be added for better discharge viewing if required in later experiments.  This is the device with which we have observed spatially uniform discharges in a potassium-argon mixture at 7 atm.  The major problem encountered with this design has been a limitation on maximum temperature of $\sim 250^{\circ}$C caused by heat loading at the mounting fixtures.

4684-13

POTASSIUM INLET

RE-ENTRANT BREWSTER'S ANGLE WINDOW ASSEMBLY

OUTER SAFETY CYLINDER STEEL

ALKALI RESISTANT GLASS SLEEVE

UV SOURCES

POTASSIUM WICK

PRESSURE VESSEL (PYREX)

SCALE
1"

GAS INLET

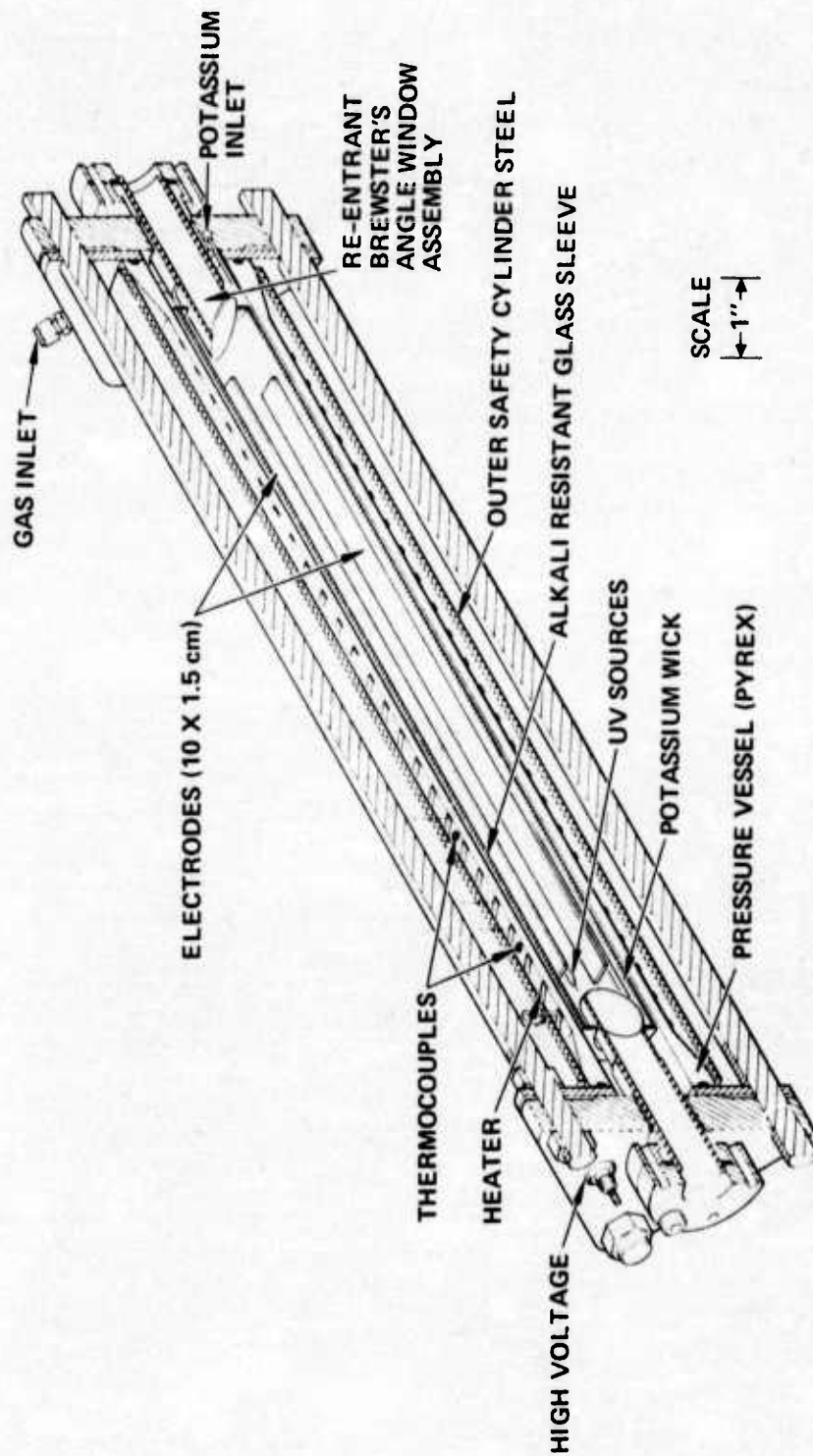ELECTRODES (10 X 1.5 cm)

THERMOCOUPLES

HEATER

HIGH VOLTAGE

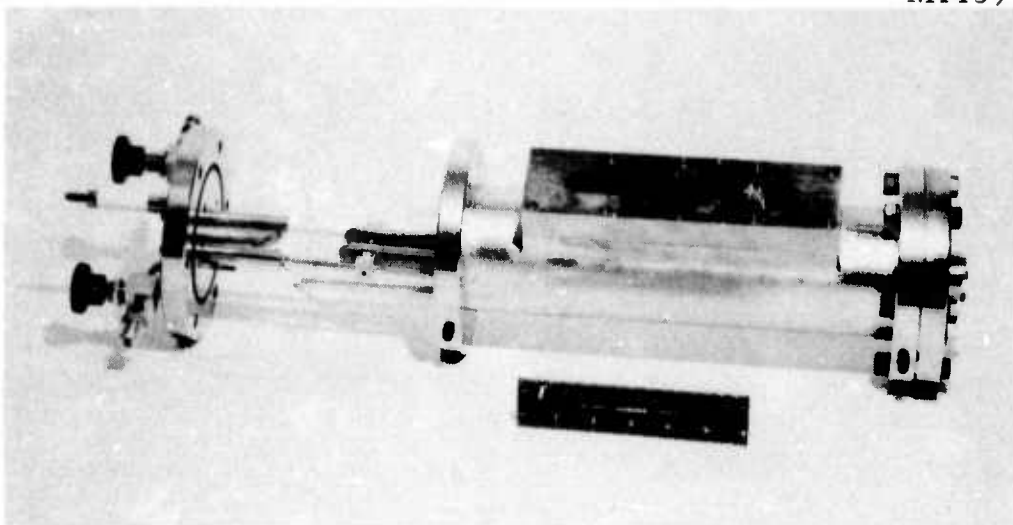Fig. III-1. Alkali-rare gas discharge tube, design - 1.

21

Fig. III-2.  Photograph of alkali-rare gas high pressure dis-
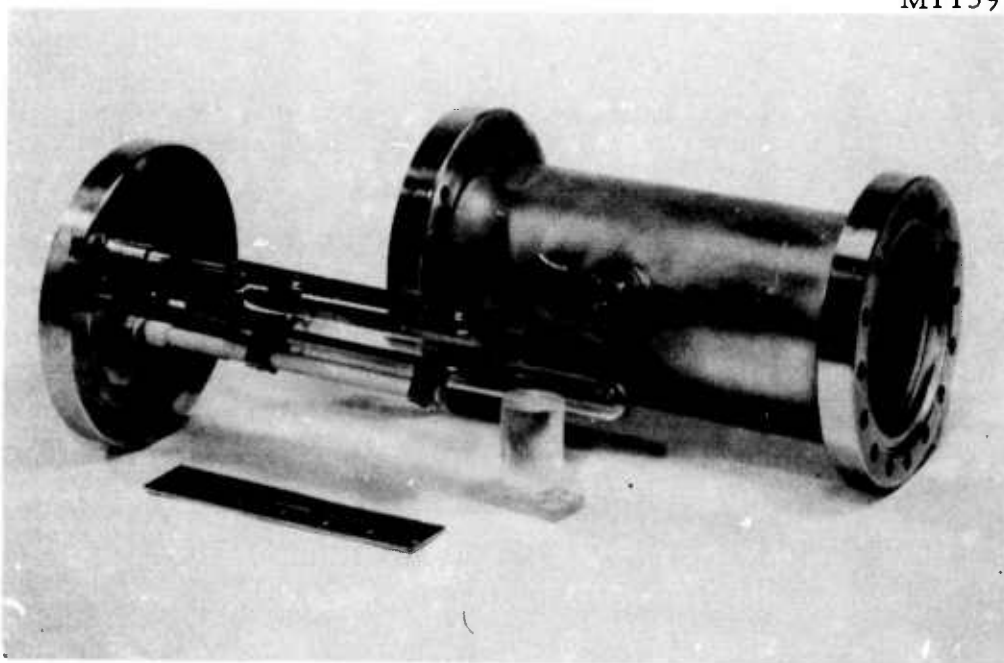charge apparatus, design 2.

Fig. III-3.  Photograph of alkali-rare gas discharge appara-
tus, design 3.

Modifications are presently underway to correct this design limitation.

The electrode profile which we have used to date is planar with the sides and ends contoured to the curvature of an ellipse. The electrode is flat over a region ~ 1.3 times the discharge gap and then joins smoothly to an ellipse. In previous work we have found the electric field between electrodes of this type to be uniform to better than 1% as determined by electrostatic potential plots using resistance paper. The present electrode profile is expected to be satisfactory as judged by our first results and is advantageous for scaling to larger sizes because of the simplicity of its shape. The major difficulty with other electrode shapes such as the Rogowskii profile is the extreme width which must be used if the central portion of the electrode is made very planar to avoid constriction of the discharge width.

B.    Aerosol Studies and Optical Measurements of Potassium

In some of our previous work with small-scale apparatus (75 $cm^3$) we have observed significant optical scattering losses in potassium-rare gas mixtures at high temperatures ($300^o$C) and pressures (10 atm). This was also found to be a problem with the large volume apparatus shown in Fig. III-2. Quantitative optical transmission measurements and qualitative side scattering observations were conducted during this reporting period with apparatus of the type shown schematically in Fig. III-4. Results of transmission measurements with a broad-band tungsten light source are illustrated in Fig. III-5. It is apparent from the data in Fig. III-5 that a large optical loss occurs over a wide wavelength region ($\approx 400$ Å) under certain experimental conditions. In addition to this transmission reduction with time, strong side scattering from a He-Ne laser beam was also observed. This experiment was conducted with the apparatus shown in Fig. III-2. Potassium was vaporized from a 0.6 cm x 15 cm stainless steel wick situated near the bottom of the housing with an argon pressure of 1 atm. Following these observations of aerosol formation in the discharge apparatus, diagnostic experiments were conducted in sealed off pyrex vessels situated in a uniform temperature muffle furnace as shown in Fig. III-6.
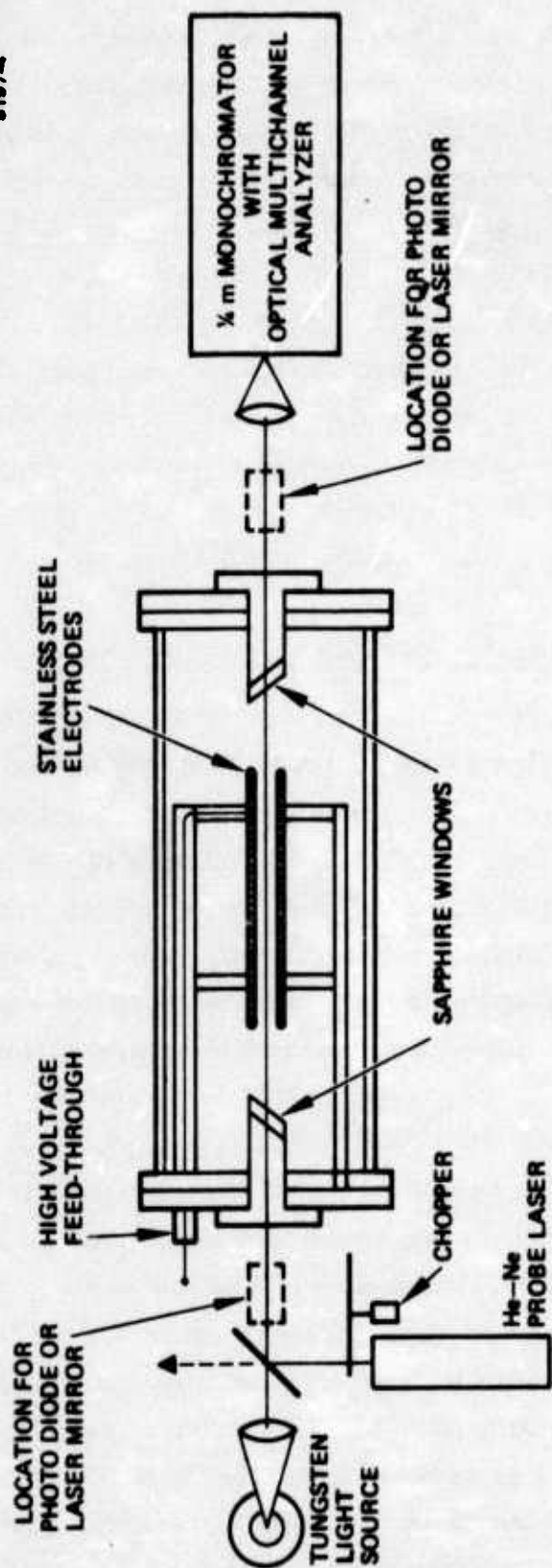
Fig. III-4.  Schematic diagram of alkali-rare gas discharge apparatus and optical monitoring equipment.

$[Ar] = 2.4 \times 10^{19} \, cm^{-3}$

$\lambda \longrightarrow$

T = 230 °C
10:30 a.m.

T = 305 °C
11:05 a.m.

7665 Å     7699 Å

T = 305 °C
1:45 p.m.

T = 305 °C
5:00 p.m.

TRANSMISSION

Fig. III-5.   Optical transmission data illustrating aerosol formation in potassium-argon mixture.

25

Fig. III-6. Schematic diagram of apparatus for optical measurements of alkali-rare gas mixture with uniform temperature control.

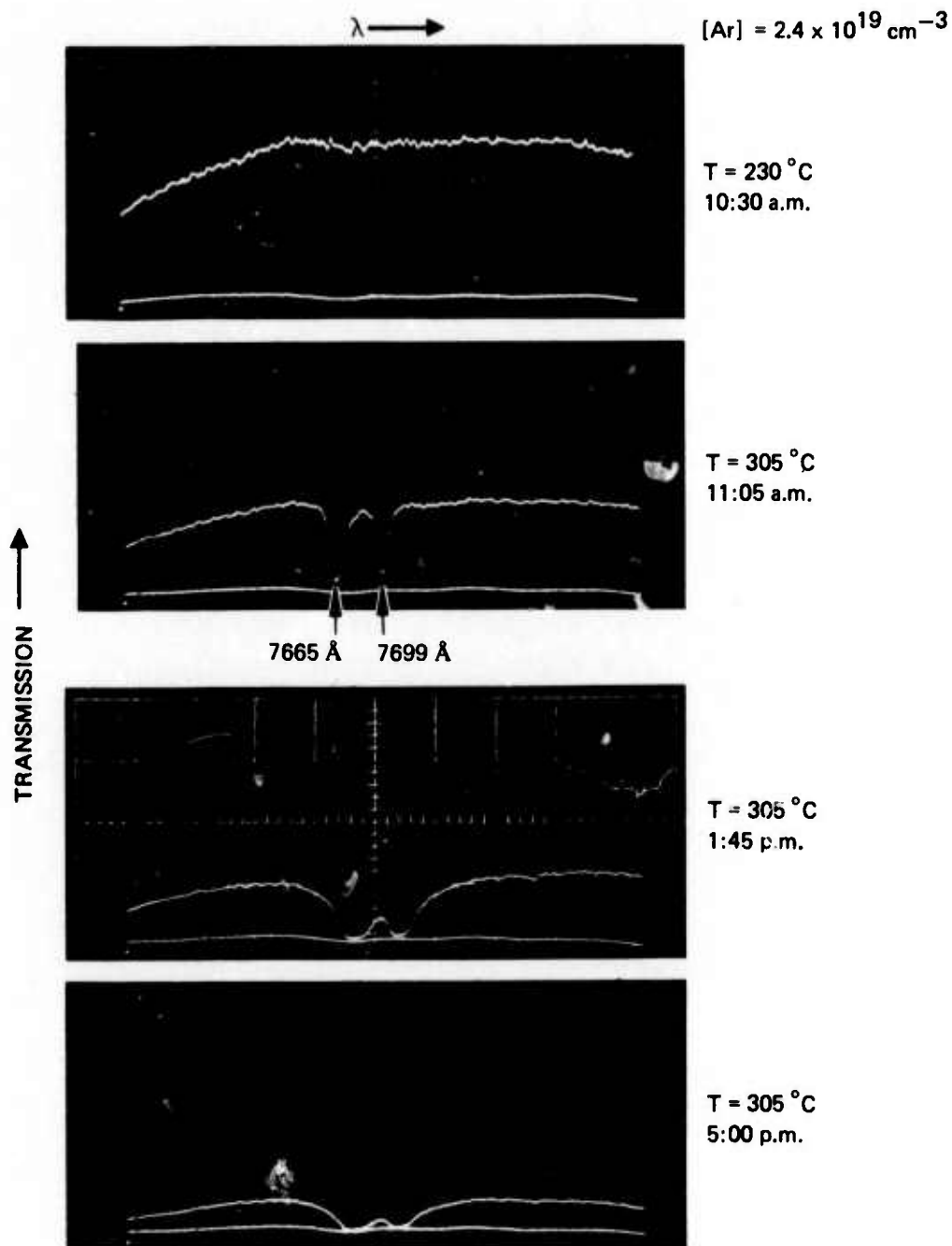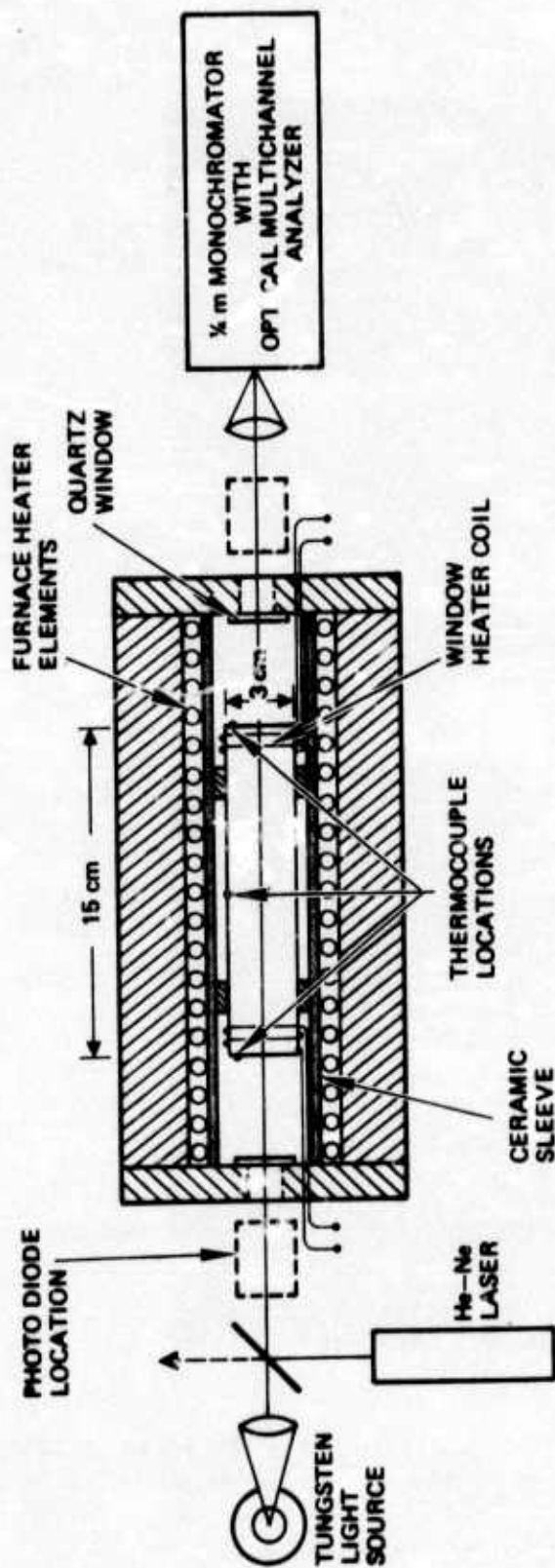Optical transmission measurements with the broad-band light source over 400 Å bandwidths centered at 7700 Å and 6475 Å at different pressures of argon were carried out along with transmission and scattering measurements with a He-Ne laser beam. The cell was filled with potassium and argon on a separate processing apparatus, sealed off and located in the furnace for optical measurements. Quantitative correlations with equilibrium atomic potassium and potassium dimer densities were observed over the temperature range of $25^\circ C$ to $350^\circ C$ and argon pressures from 0 to 2 atm; experiments were not conducted at higher argon pressures in this apparatus. A comparison between our measured values of potassium dimer absorption coefficient and those of Lapp and Harris[8] is shown in Fig. III-7. Using their value of 20 $Å^2$ for the absorption cross section of $K_2$ at 6465 Å and our measured absorption coefficient of 0.098 $cm^{-1}$ at $325^\circ C$, we obtain a potassium dimer density of $4.9 \times 10^{13}$ $cm^{-3}$ which compares very favorably with the density of $5.0 \times 10^{13}$ $cm^{-3}$ calculated from equilibrium vapor pressure data[9]. It is more difficult to deduce atomic densities of potassium from optical absorption measurements at high temperatures and pressures because of the complex optical broadening mechanisms involved; a well documented curve of growth for the integrated absorption under these conditions has not been established. However, since we have obtained good agreement between equilibrium values of potassium dimer densities and our measurements, it is reasonable to infer that equilibrium between atomic and dimeric potassium is attained in our apparatus. Thus we will obtain atomic potassium densities from measurements of dimeric potassium under conditions where the dimer spectrum is pressure broadened into a continuum.

No aerosol formation was observed during the experiments conducted in this apparatus. This is illustrated by the optical transmission data shown in Fig. III-8 which was obtained under the carefully controlled conditions described above. Note the dramatic contrast between this data and that shown previously in Fig. III-5. We conclude that equilibrium values of potassium vapor density can be obtained in argon at temperatures up to $350^\circ C$ and pressures up to 2 atm if the

5197-22

(a)

100% TRANSMISSION
BASELINE

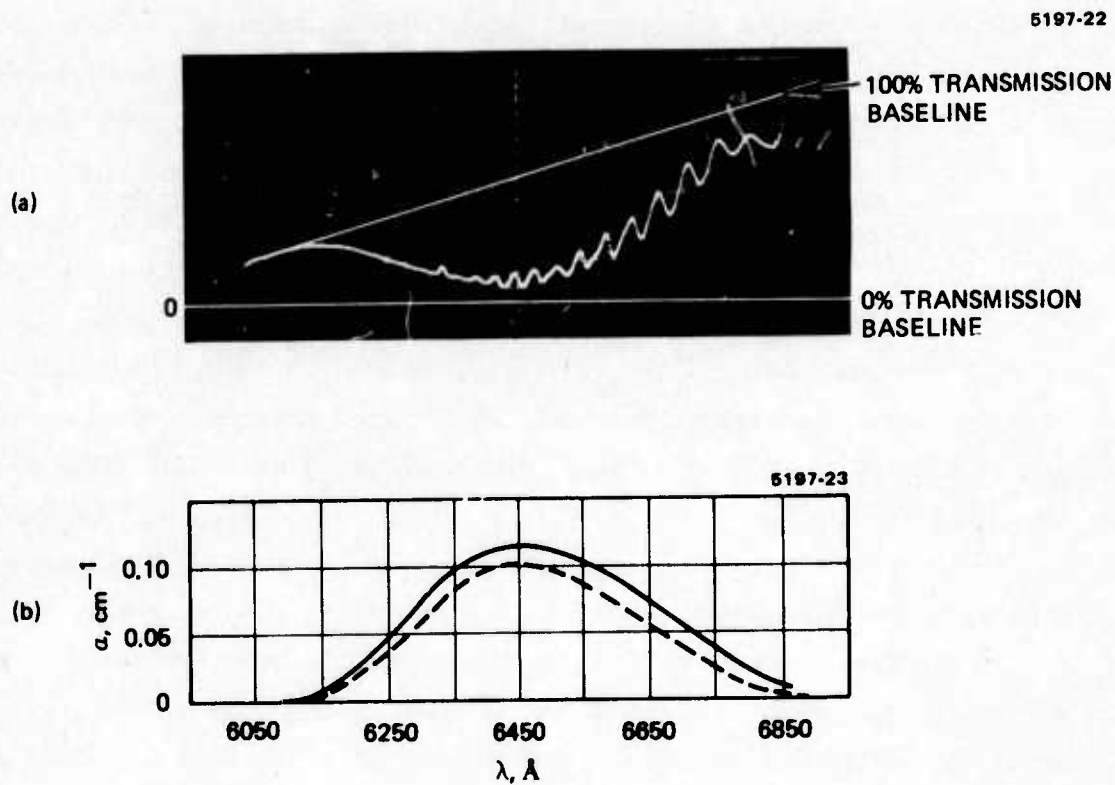0% TRANSMISSION
BASELINE

5197-23

(b)

Fig. III-7.   Potassium dimer.  (a) Optical transmission, and
(b) absorption coefficient.  Solid curve is from
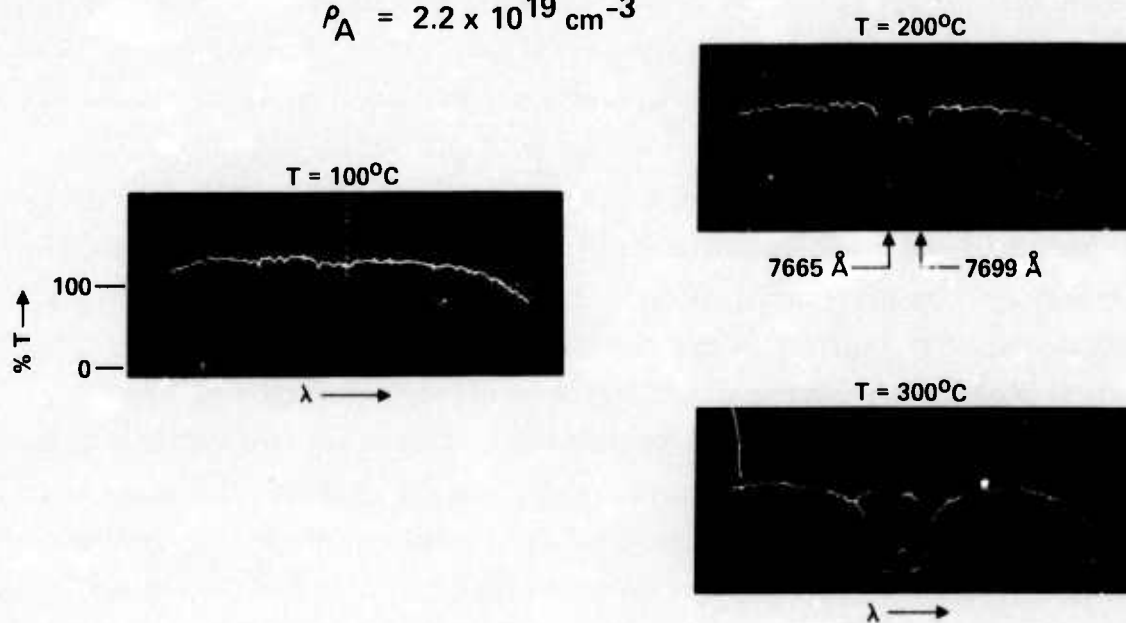Reference 8, dashed curve is our measurement.

Fig. III-8.   Optical transmission through potassium-argon in 15 cm
sealed off cell.

temperature of the apparatus is kept uniform. This is considerably more difficult in the discharge system without incorporating elaborate heating equipment because of the uneven heat capacity of the internal parts of the discharge chamber. We infer that potassium aerosols form when macroscopic size volumes of saturated vapor densities come in contact with cold spots inside the discharge chamber. In the region around these cold spots the saturated vapor density is transformed to a super-saturated vapor through heat transfer to the colder region. The super-saturated vapor is subsequently converted to an equilibrium vapor by condensation into macroscopic particles of liquid potassium. High pressures of inert gas in a large diameter chamber contribute to the aerosol formation by increasing the diffusion time of the alkali vapor and thereby preventing it from maintaining a dynamic equilibrium with the coldest regions in the chamber.

With this hypothesis and our experience with the sealed-off cells in the uniform oven, we postulated that aerosols could be eliminated in the large discharge apparatus by slowly evolving the potassium vapor in the absence of inert gas and then mixing pre-heated gas with the alkali vapor after equilibrium vapor densities of the pure metal vapor were obtained. Experiments were performed following this procedure by pre-heating argon to a temperature 50 degrees higher than the temperature of the discharge chamber. Uniform mixing was achieved by admitting the gas into the potassium vapor by means of a perforated stainless steel sting. The results of this set of experiments are summarized by the optical transmission data in Fig. III-9 taken with the apparatus as shown schematically in Fig. III-4. No aerosol formation occurred as indicated by this data and by the complete absence of scattering from the He-Ne laser beam. Thus, we have arrived at an experimental procedure for obtaining homogeneous mixtures of alkali vapors and rare gases at high temperatures ($300^\circ$C) and pressures (7 atm). These values of temperature and pressure are by no means expected to be upper limits but rather reflect the range over which carefully controlled experiments have been conducted in apparatus of the type necessary for alkali-rare gas excimer laser systems.
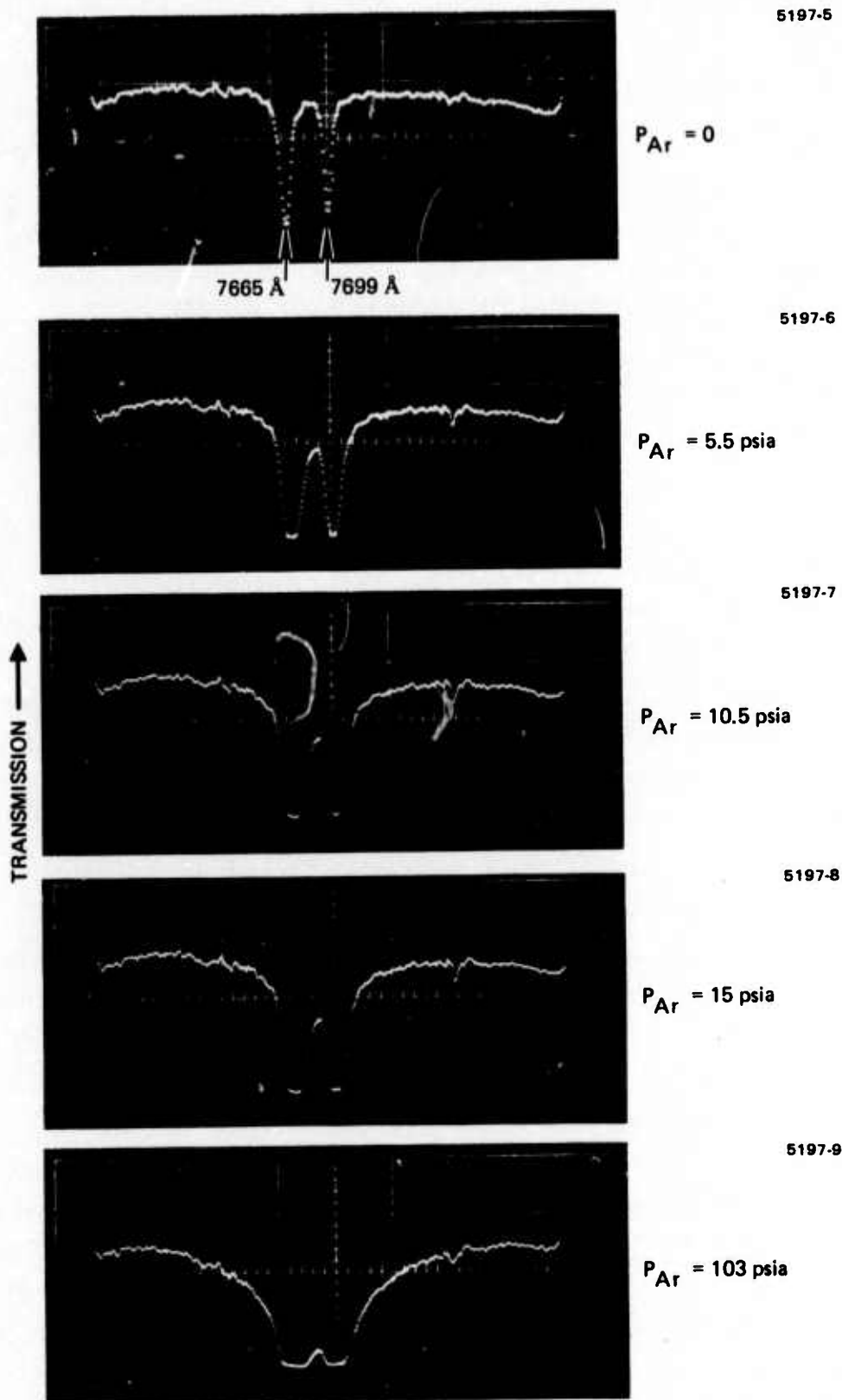
30

Fig. III-9.  Optical transmission through the discharge apparatus indicating no aerosol formation. (T = 300°C).

31

C.    Electrical Discharge Experiments

After establishing an aerosol-free mixture of potassium vapor and argon at 7 atm pressure, electrical discharge measurements were initiated. Using this argon density ($9 \times 10^{19} cm^{-3}$) and an indicated oven temperature of $300^{o}C$, a variety of experiments were conducted to evaluate both the electrical and optical characteristics of the discharge. Qualitative visual observations of the discharge through the 1.5 cm side viewing window and through the end windows indicated that we had achieved a very uniform diffuse discharge over the entire electrode area without the use of any discharge preconditioning.

This is partially illustrated by photographs of the discharge through the side window shown in Fig. III-10. The field of view of the camera used here is considerably smaller than the full discharge region and also smaller than a person's eye located adjacent to the side window. Two exposure levels are shown to verify the lack of small scale striations in the discharge. As far as can be ascertained, the discharge is very uniform under the operating conditions of temperature and pressure utilized here ($300^{o}C$, 7 atm Argon).

Voltage and current characteristics of this pulsed discharge operating without preionization are shown in Figs. III-11 and III-12. A negative voltage is applied across the electrodes by means of a thyratron switching tube and a capacitor previously charged to a particular voltage level. The current pulse develops after a delay time of a few microseconds and has a time duration which is dictated by the self-inductance and capacitance of the circuit rather than the plasma impedance. As the applied voltage is increased, breakdown occurs at earlier times and the peak current increases in proportion to the charge initially stored on the capacitor. This variation in time between application of the voltage and development of the current is not visible in Figs. III-11 and III-12 because the complete time interval of the experiment can not always be displayed on the time scale chosen to fully resolve the current pulses. Considerable power loading into the discharge has been achieved ($\sim 10$ kW/cm$^3$) without development of an arc. When the temperature is decreased by $25^{o}C$ from the indicated

5197-11

(a)

5197-12

(b)
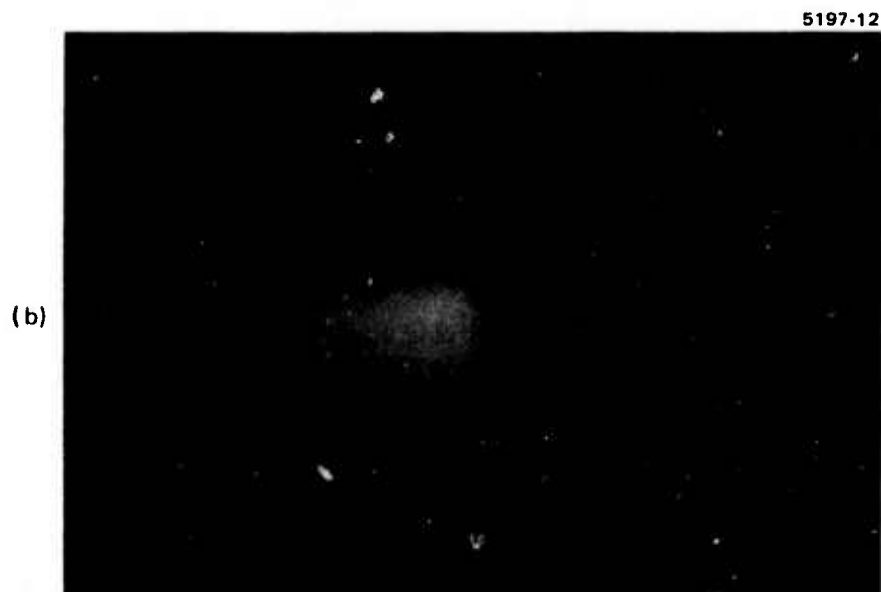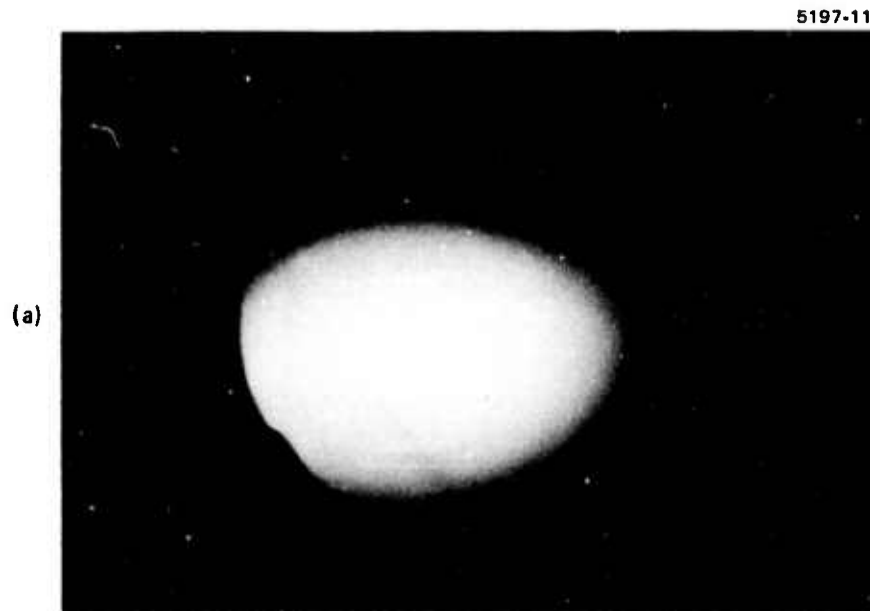
Fig. III-10.  Photograph of potassium-argon discharge
as viewed through the 1.5 cm side win-
dow.  Film exposure of (b) is 5 times
less than (a).

**5197-13**

(a)

$V_0 = 4.5$ kV
$C = 2.7$ nF

**5197-14**

(b)

$V_0 = 8$ kV
$C = 2.7$ nF

Fig. III-11.   Current-voltage waveform
characteristics of potassium-
argon transverse discharge.
Upper traces — voltage,
lower traces — current.
Sensitivities:  (a) 5 kV/cm,
20 A/cm; (b) 5 kV/cm,
50 A/cm.

34

5197-15

(a)

$V_0 = 5 \text{ kV}$

$C = 0.01 \mu\text{F}$

5197-16

(b)

$V_0 = 8 \text{ kV}$

$C = 0.01 \mu\text{F}$

Fig. III-12. Current-voltage character-
istics of potassium-argon
discharge. Upper traces —
voltage, lower traces —
current. Sensitivities:
(a) 5 kV/cm, 50 A/cm;
(b) 5 kV/cm, 200 A/cm.

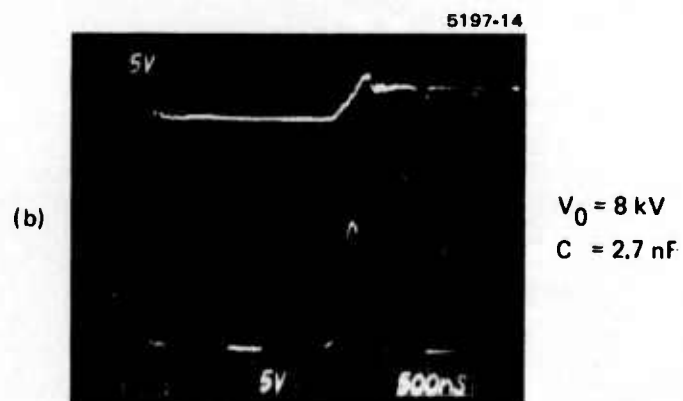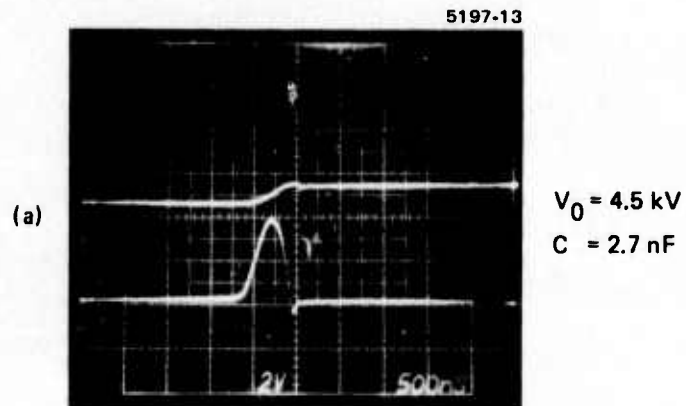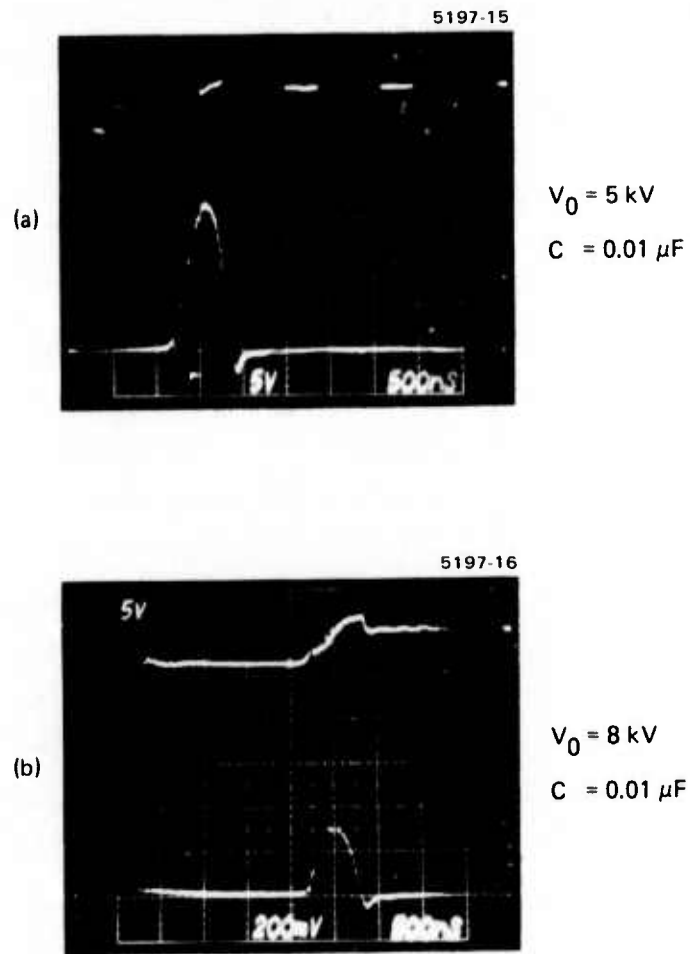temperature of 300°C, arcing does occur approximately 50% of the time and arcs were observed occasionally at voltages near 9 kV. However, the latter case may be simply related to an internal breakdown through the high voltage feedthrough to ground rather than across the electrodes. Minor changes in the apparatus are presently being made in order to prevent this possibility in future work. A few experiments were also carried out using a quartz flashlamp for pre-ionization of the discharge. The results have not been examined in detail but we note here that the time interval between discharge current onset and voltage application decreases markedly (several microseconds) with increasing flashlamp intensity.

In addition to characterization of the electrical features of the discharge, we have also conducted spectroscopic investigations of the optical emission at wavelengths from 7400 Å to 1.1 μm. An emission spectrum in the wavelength region near the potassium-argon excimer band is shown in Fig. III-13(a). Self-absorption by ground state potassium in the region between the electrodes and Brewster angle windows is responsible for the two negative peaks at 7665 Å and 7669 Å. The length of this optical loss region will be reduced from the present 5 cm to ~1 cm during the device modifications that are currently in progress. Another spectrum is shown in Fig. III-13(b) with an intensity scale 2.5 times more sentitive than in Fig. III-13(a) which demonstrates the large bandwidth and spectral shape of the excimer emission. The emission peak at 8085 Å has not been specifically identified, but may be a result of impurities in the system. No emission could be detected at wavelengths greater than 8700 Å although strong potassium dimer emission is expected at 1.04 μm. After a thorough search for the dimer emission, we dismantled the discharge apparatus and found that potassium metal had condensed near one of the system mounting posts. This suggests that the coldest position in the apparatus was at this location and was significantly lower in temperature due to heat transfer through the mounts than indicated by the probe thermocouple located in a quartz tube near the center of the electrode regions. Ten other thermocouples were located throughout the apparatus and these
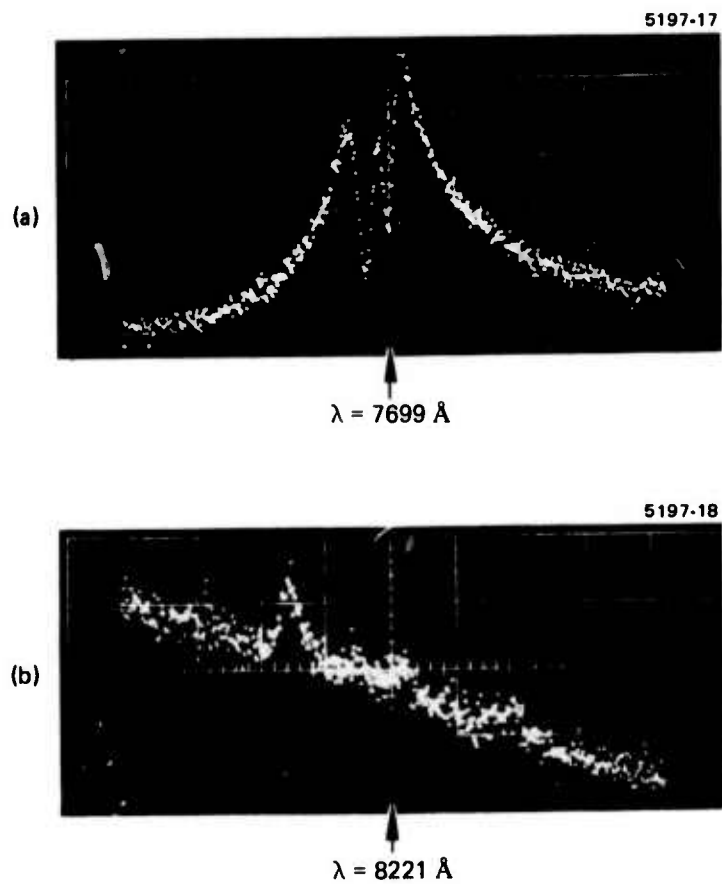
36

5197-17

(a)

λ = 7699 Å

5197-18

(b)

λ = 8221 Å

Fig. III-13.  Potassium-argon excimer
emission.  Sensitivity of (b) is
2.5 times that of (a).  Wave-
length scale — 100 Å/cm.

37

positions were always maintained at higher temperatures than the probe thermocouple in the quartz tube. Moreover, after these discharge measurements were made, we carefully monitored the optical transmission of a He-Ne laser beam through the discharge apparatus. This data is presented in Fig. III-14. In addition to a residual optical loss at the end windows, the onset of absorption occurs at a measured temperature which is $50^o$ higher than the calculated temperature for absorption onset based on equilibrium vapor pressure data. The actual or effective gas temperature is clearly considerably lower than indicated by the thermocouple in the quartz probe tube. Thus we conclude at this time that the discharge measurements to date in this apparatus have been made at temperatures which may be $50^oC$ or more lower than measured directly. This does not reduce the significance of the results obtained but mandates equipment modifications before potassium vapor densities high enough to achieve optical gain can be obtained. We are now in a position to accurately monitor atomic potassium through optical measurements of potassium dimer concentrations since we have experimentally demonstrated a correlation with our measurements and equilibrium vapor pressure data of both these species (see Fig. III-7 and the discussion in Section III-B).

An additional experimental observation on the discharge emission is shown in Fig. III-15 where it is seen that the excimer emission in the 7700 Å region closely follows the temporal behavior of the discharge current pulse. In Fig. III-16 is shown a comparison between the potassium-argon excimer emission and absorption which illustrates, along with Fig. III-13(b), the extension of the long wavelength excimer emission beyond the absorption region. It is in this spectral region where the excimer emission is strong compared to absorption and consequently where optical gain can be obtained.
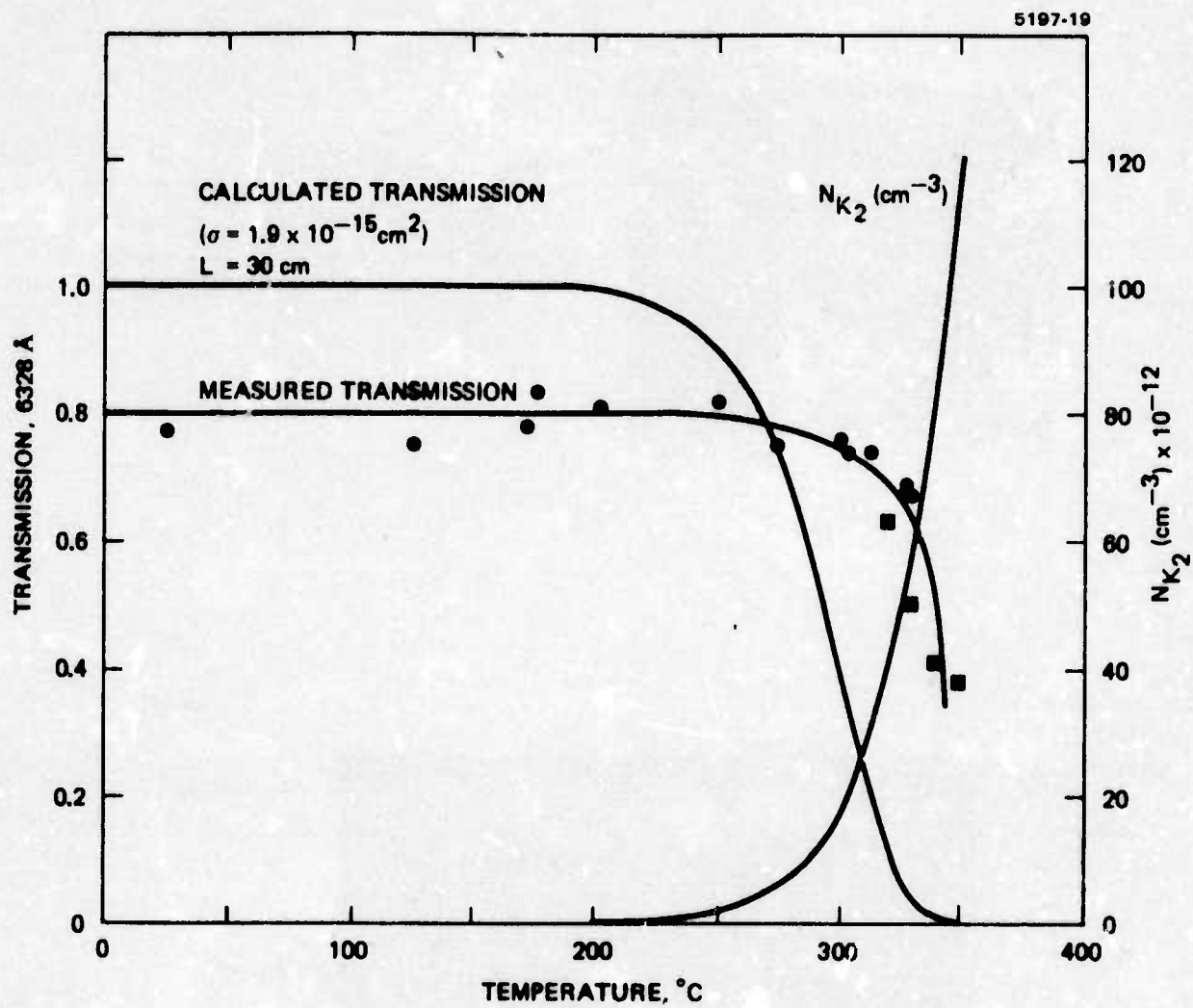
38

5197-19

Fig. III-14. Potassium dimer concentration and optical transmission at 6328 Å.

5197-20

Fig. III-15.
Temporal profiles of
potassium-argon excimer
emission (upper trace) and
discharge current (lower
trace).



5197-21

TRANSMISSION

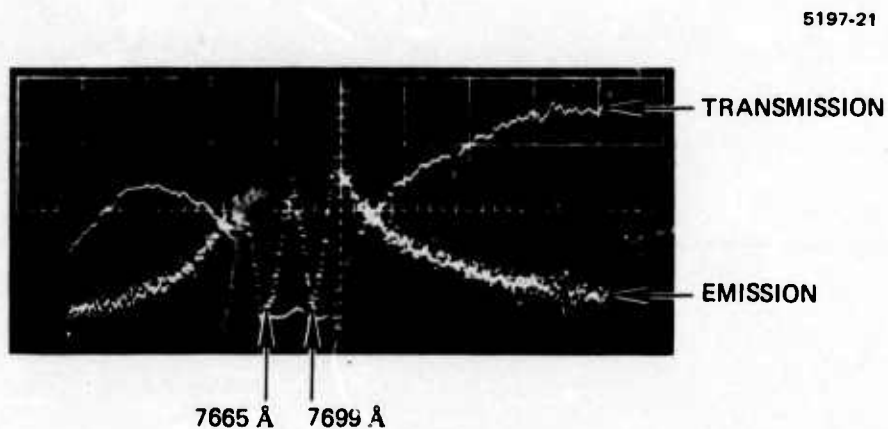EMISSION

7665 Å     7699 Å

Fig. III-16.   Superposition of potassium-argon excimer
optical emission and transmission spectra.

## IV.    FUTURE WORK PLAN

All theoretical and experimental efforts during the next six-month period will be directed toward achieving laser oscillation on either the K-Xe or K-Ar Z-X excimer transition or the A-X $K_2$ dimer transition from the present transverse discharge apparatus.

Modifications to the experimental discharge apparatus which will allow the achievement of potassium densities up to $10^{16}$ cm$^{-3}$ are presently in progress. Additionally, a new set of electrodes having a length of 25 cm is being fabricated which represents an increase in optical gain path of 11.5 cm over the previous electrodes.

Theoretical modeling will concentrate on guiding the experiments into operating regimes which appear to provide the highest laser gain under conditions generally being achieved in the laboratory. Up-grading of the modeling will be carried out continuously through the incorporation of cross-section and rate constant data being obtained or inferred through measurements here and elsewhere. Also, the Maxwellian electron distribution used at present will either be quantitatively justified or replaced by either a solution to the Boltzmann equation or a two-group Maxwellian distribution.[10] Stimulated emission processes will be added to the model when appropriate for interfacing with the experiments.

# REFERENCES

1. A. von Engel, _Ionized Gases_ (Oxford Clarendon Press, 1965).

2. A.J. Palmer, _Excimer Lasers_, Semiannual Technical Report for 1 April 1975 - 30 Sept. 1975, Contract N00014-75-C-0081, Hughes Research Laboratories, December 1975.

3. L.J. Kieffer, JILA Information Center Report No. 13, University of Colorado, Sept. 30, 1973.

4. Geoffrey V. Marr, "Photoionization Processes in Gases" Academic Press, 1967.

5. S.C. Brown, _Basic Data of Plasma Physics_ (The MIT Press, 1967).

6. G. York and A. Gallagher, JILA Report No. 114, University of Colorado, (Oct. 15, 1974).

7. R.E.M. Hodges, D.L. Drummond, and A. Gallagher, Phys. Rev. A 6, 1519 (1972).

8. M. Lapp and L.P. Harris, J. Quant. Spectrosc. Radiat. Transfer. 6, 169 (1966).

9. _Thermodynamic Properties of the Elements_, compiled by D.R. Stull and G.C. Sinke, Adv. Chem. Ser. No. 18 (1956).

10. L. Vriens, J.A.P. 45, No. 3, 1191 (1974).

```
C KXECP - PULSED K-XE LASER
      REAL MASE,MASXE,MASM,M1,M2,MI,K,K3X,K5X,K41,NEO,NE
      REAL LAMDE,LAMDD,KAEX,KADI,KXEX,KXDI
      REAL NEP
      REAL J
      REAL LENGTH
      REAL KPLUS,KNI,KEL
      REAL L
      EXTERNAL FUNC
      COMMON/STOR/XE,PO,CPI,CXI,NE,NEP,L,A,R,DT,E,
     + EPI,EXI,CEL,MASE,MASXE,V,LENGTH,PI,CPII,CPI,EPI
      COMMON/STE/TE
C CONSTANT DATA (DATA IS FOR K-XE)
      MASE=0.5E6; E=1.6E-19; MASXE=131*1840*.5E6
      R=0
      C=2.7E-9
      D=1
      A=27
      LAMDE=.85E-4
      LAMDD=1.04E-4
      AP=3.69E7
      REX=3.7E-8
      RDI=5.4E-8
      RDIE=4.4E-8
      DRDFE=.53E-8/(579)
      DRDFD=1E-8/(.04E4)
      DRDFDE=.4E-8/(1.388E3)
      VEA=-.079
      VEX=.062
      VDA=-.66
      VDX=-.262
      VDXE=-.560
      EPI=1.61
      EPI=4.34
      EPXI=1.46
      EPXI=4.19
      EPDI=1.46
      EPDI=4.19
      CPI=6E-15
      CPI=.5E-16
      CPII=5E-16
      CPHI=.05E-18
      CEL=5.5E-16
      CDIF=1E-15
      SA=8.49E4;SB=7.18
      LENGTH=1
      K=160E19
```

45

```
      AX2=4E7;AP=3.69E7;AXEDI=4E7
      CSTME=AP/2*LAMDE**2*REX**2*DRDFE
      CSTMD=AP/2*LAMDD**2*RDI**2*DRDFD
      CSTMDE=AP/2*LAMDE**2*RDIE**2*DRDFDE

C INITIAL CONDITIONS
      WRITE(5, 50)
   50 FORMAT(2X,2HXE,2X,2HTG,2X,1HW,2X,1HV,2X,1HC,2X,2HDT,2X,6HIPRINT,
     +2X,4HTMAX,2X,5HDELAY)
      ACCEPT*,XE,TG,W,V,C,DT,IPRINT,TMAX,DELAY
      PO=2.7E16*(273/(273+TG))*10**(SB-.052*SA/(TG+273))
      TG=(TG+273)*(1/1.16E4)
      TGO=TG
      F=W/(1.6E-19*EPI)*(1.24/EPI-.2)
        KXDI=1.8E-22*EXP(.56/TG)
      KXEX=2.2E-23*EXP(-.05/TG)
      PX=KXEX*PO*XE
      PD=KXDI*PO**2
      PX=KXEX*PO*XE
      PI=F*CPHI*PO*DELAY
      PI=10.*PI
      AT=AP*1.6/(8.3E-15*PO*D)
      IF(AT-AP) 18,17,17
   17 AT=AP
   18 CONTINUE
      WRITE(5, 82) PO,PD,PI
   82 FORMAT(2X,'PO=',E10.3,5X,'PD=',E10.3,5X,'PI=',E10.3)
      WRITE(5, 80)
   80 FORMAT(4X,4HTIME,6X,5HVDISC,5X,1HJ,9X,2HNE,8X,2HPI,
     +8X,3HPXI,7X,3HPDI)
      WRITE(5, 85)
   85 FORMAT(7X,1HP,9X,2HPI,8X,5HGAINE,5X,5HGAIND,5X,5HBETAE,5X,5HBETAD,
     +5X,2HTE)
C TIME STEP
   20 ISTEP=ISTEP+1
      T=T+DT
      IF(T-TMAX) 21,21,22
   21 CONTINUE
C CIRCUIT RESPONSE
      P=PO-(PI+PI)
      NE=PI
      V=V-DT*J*A/C
      IERR=0;IND=1;EPS=0.01
      TE=SOLN(IND,FUNC,.1,5.,EPS,IERR)
      IF(IERR) 1,2,1
    1 WRITE(5,*) IERR;GO TO 30
      STOP
    2 CONTINUE
```

```
C RATE CONSTANTS - ELCTRONIC
      VD=SQRT(2*TE/MASXE)*3E10
      J=NE*E*VD
      VDISC=V-R*J*A-L*A*E*VD*(NE-NEP)/DT
      NEP=NE
      RC=6.38E7*(SQRT(2*TE))**3
      RPI=RC*EXP(-EPI/TE)*(1+EPI/(2*TE))*(NE*CPI)*P
      RPIB=RPI/P*EXP(EPI/TE)*PI*.33
      RPI=RFN(EPI)*(NE*CPI)*P
      RPII=RFN(EPI-EPI)*(NE*CPII)*PI
      RECP=PI*2.28E-26*NE*TE**(-4.39)*NE
      RECPX=3.3E-5*TE**(-.67)*PXI*NE
      RECPD=3.3E-5*TE**(-.67)*PDI*NE
C RATE CONSTANTS - GAS KINETIC
      SQRTG=SQRT(TG)
      KAEX=2.2E-23*EXP(.074/TG)
      KADI=6.5E-23*EXP(.735/TG)
      KXEX=2.2E-23*EXP(-.05/TG)
      KXDI=1.8E-22*EXP(.56/TG)
      GPX=XE*8E-32*XE*PI
      GPXB=XE*8E-32/KAEX
      GPD=P*(XE*8E-30*PI)
      GPDB=(XE*8E-30)/KADI
      GPXI=(XE*8E-32*XE)*PI
      GPXIB=(XE*8E-32*PXI)/KAEX
      GPDI=(XE*8E-30*P)*PI
      GPDIB=(XE*8E-30*PDI)/KADI
C DIFFUSION RATES
      KPLUS=2E3*(3E16/(XE))*SQRT(.03/TG)
      KEL=VD/(VDISC/LENGTH)
      DXE=SQRT(2*TG/MASXE)*3E10/(3*(XE)*CDIF)*(4.8/D)**2
      DAPOS=KPLUS*TE*(4.8/D)**2
      DP=DXE*1.8
C RATE EQUATIONS
      PI=PI+DT*(RPI+RECP+RECPX+RECPD-RPIB-AP*(PXI+PDI)-DP*PI)
      IF (PI/P-3*EXP(-EPI/TE)) 8,9,9
    9 PI=P*3*EXP(-EPI/TE)
    8 CONTINUE
      PX=KXEX*P*XE
      PD=KXDI*P**2
      PI=PI+DT*(RPI+RPII+RP2I+GPN*P+P*CPHI*F-RECP-RECPX-RECPD-DAPOS*PI)
      PXI=GPX/(GPXB+AP)
      PXI=KAEX*PI*XE
      PDI=GPD/(GPDB+AP)
      PDI=KADI*P*PI
C GAS TEMPERATURE
      TG=TG+DT*(NE*VD*VDISC/LENGTH-(4.8/D)**2*K*(TG-TGO))*2/(3*XE)
```

```
C GAIN
      BETAE=CSTME*2*P*XE*EXP(-VEX/TG)/3E10+CSTMDE*P**2*EXP(-VDXE/
     +TG)*.25/3E10
      BETAD=CSTMD*P**2*EXP(-VDX/TG)*.25/3E10
      GAINE=CSTME*(PX1*EXP(-VEA/TG)/(KAEX*1.5)-2*P*XE*EXP(-VEX/TG))/3E10
     +-CSTMDE*(P**2*EXP(-VDXE/TG)*.25)/3E10
      GAIND=CSTMD*(PD1*EXP(-VDA/TG)/(KADI*12)-P**2*EXP(-VDX/TG)*.25)
     +/3E10
C OUTPUT
      IF(ISTEP/IPRINT-FLOAT(ISTEP)/FLOAT(IPRINT)) 31,30,31
   30 CONTINUE
      WRITE(5,*) TG
      WRITE(5,90) T,VDISC,J,NE,PI,PX1,PD1
   90 FORMAT( 7(E10.2))
      WRITE(5, 95) P,PI,GAINE,GAIND,BETAE,BETAD,TE
   95 FORMAT(3X,7(E10.2))
   31 CONTINUE
      GO TO 20
   22 WRITE(5, 200)
  200 FORMAT( 2X,19H>0, GO ON---<0, END)
      ACCEPT*,Z
      IF(Z ) 41,41,42
   42 WRITE(5, 250)
  250 FORMAT(2X,28HNEW VALUES: DT, TMAX, IPRINT, F)
      ACCEPT*,DT,TMAX,IPRINT,F
      ISTEP=0
      GO TO 20
      STOP
   41 END
      FUNCTION FUNC(TE)
      REAL NE,MASE,MASXE,LENGTH,NEP,L
      COMMON/STOR/XE,PO,CP1,CX1,NE,NEP,L,A,R,DT,E,
     + EP1,EX1,CEL,MASE,MASXE,V,LENGTH,P1,CP11,CPI,EPI
      VD=SQRT(2*TE/MASXE)*3E10
      RC=6.38E7*(SQRT(2*TE))**3
      RP1=RC*EXP(-EP1/TE)*(1+EP1/(2*TE))*CP1*PO
      REL=(CEL*XE*SQRT(2*TE/MASE))*3E10*(2*MASE/MASXE)*TE
      FUNC=(V-R*A*E*NE*VD-L*A*E*VD*(NE-NEP)/DT)/LENGTH
     + -(1/VD)*(RP1*EP1+REL)
      RETURN;END
      FUNCTION RFN(Y)
      COMMON/STE/TE
      RFN=6.38E7*(SQRT(2*TE))**3*EXP(-Y/TE)*(1+Y/(2*TE))
      RETURN;END
```

48